

Search for Resonant $B^\pm \rightarrow K^\pm h \rightarrow K^\pm \gamma\gamma$ Decays at Belle

Belle Collaboration

J. Wicht^p, I. Adachi^g, H. Aihara^{ao}, D. Anipko^a,
 V. Aulchenko^a, T. Aushev^{p,k}, A. M. Bakich^{aj}, E. Barberio^s,
 I. Bedny^a, U. Bitenc^ℓ, I. Bizjak^ℓ, A. Bondar^a, A. Bozek^x,
 M. Bračko^{g,r,ℓ}, J. Brodzicka^x, T. E. Browder^f, P. Chang^w,
 Y. Chao^w, A. Chen^u, W. T. Chen^u, B. G. Cheon^e, I.-S. Cho^{at},
 Y. Choi^{ai}, Y. K. Choi^{ai}, J. Dalseno^s, M. Dash^{as}, S. Eidelman^a,
 D. Epifanov^a, S. Fratina^ℓ, A. Go^u, A. Gorišek^ℓ, H. Haⁿ,
 T. Hara^{ac}, K. Hayasaka^t, M. Hazumi^g, D. Heffernan^{ac},
 L. Hinz^p, Y. Hoshi^{am}, W.-S. Hou^w, Y. B. Hsiung^w,
 H. J. Hyun^o, K. Ikado^t, K. Inami^t, A. Ishikawa^{ao}, H. Ishino^{ap},
 M. Iwasaki^{ao}, Y. Iwasaki^g, C. Jacoby^p, D. H. Kah^o, H. Kaji^t,
 J. H. Kang^{at}, P. Kapusta^x, H. Kawai^b, T. Kawasaki^z,
 H. Kichimi^g, H. J. Kim^o, S. K. Kim^{ah}, Y. J. Kim^d,
 K. Kinoshita^c, S. Korpar^{r,ℓ}, P. Križan^{q,ℓ}, P. Krokovny^g,
 R. Kumar^{ad}, C. C. Kuo^u, A. Kuzmin^a, Y.-J. Kwon^{at},
 J. S. Lee^{ai}, M. J. Lee^{ah}, S. E. Lee^{ah}, T. Lesiak^x, J. Li^f,
 A. Limosani^g, S.-W. Lin^w, D. Liventsev^k, G. Majumder^{ak},
 F. Mandl^j, T. Matsumoto^{aq}, A. Matyja^x, S. McOnie^{aj},
 T. Medvedeva^k, H. Miyake^{ac}, H. Miyata^z, Y. Miyazaki^t,
 R. Mizuk^k, D. Mohapatra^{as}, G. R. Moloney^s, E. Nakano^{ab},
 M. Nakao^g, S. Nishida^g, O. Nitoh^{ar}, S. Ogawa^{al}, T. Ohshima^t,
 S. Okuno^m, Y. Onuki^{af}, P. Pakhlov^k, G. Pakhlova^k,
 C. W. Park^{ai}, H. Park^o, K. S. Park^{ai}, R. Pestotnik^ℓ,
 L. E. Piilonen^{as}, F. J. Ronga^g, Y. Sakai^g, T. Schietinger^p,
 O. Schneider^p, J. Schümann^g, K. Senyo^t, M. E. Sevior^s,
 M. Shapkinⁱ, C. P. Shen^h, H. Shibuya^{al}, J. B. Singh^{ad},
 A. Somov^c, S. Stanič^{aa}, M. Starič^ℓ, H. Stoeck^{aj},

T. Sumiyoshi ^{aq}, F. Takasaki ^g, M. Tanaka ^g, G. N. Taylor ^s,
Y. Teramoto ^{ab}, X. C. Tian ^{ae}, I. Tikhomirov ^k, T. Tsukamoto ^g,
S. Uehara ^g, Y. Unno ^e, S. Uno ^g, P. Urquijo ^s, Y. Ushiroda ^g,
Y. Usov ^a, G. Varner ^f, K. E. Varvell ^{aj}, K. Vervink ^p, S. Villa ^p,
A. Vinokurova ^a, C. H. Wang ^v, P. Wang ^h, Y. Watanabe ^{ap},
R. Wedd ^s, E. Won ⁿ, B. D. Yabsley ^{aj}, A. Yamaguchi ^{an},
Y. Yamashita ^y, Z. P. Zhang ^{ag}, V. Zhilich ^a, A. Zupanc ^l, and
N. Zwahlen ^p,

^a*Budker Institute of Nuclear Physics, Novosibirsk, Russia*

^b*Chiba University, Chiba, Japan*

^c*University of Cincinnati, Cincinnati, OH, USA*

^d*The Graduate University for Advanced Studies, Hayama, Japan*

^e*Hanyang University, Seoul, South Korea*

^f*University of Hawaii, Honolulu, HI, USA*

^g*High Energy Accelerator Research Organization (KEK), Tsukuba, Japan*

^h*Institute of High Energy Physics, Chinese Academy of Sciences, Beijing, PR China*

ⁱ*Institute for High Energy Physics, Protvino, Russia*

^j*Institute of High Energy Physics, Vienna, Austria*

^k*Institute for Theoretical and Experimental Physics, Moscow, Russia*

^l*J. Stefan Institute, Ljubljana, Slovenia*

^m*Kanagawa University, Yokohama, Japan*

ⁿ*Korea University, Seoul, South Korea*

^o*Kyungpook National University, Taegu, South Korea*

^p*École Polytechnique Fédérale de Lausanne (EPFL), Lausanne, Switzerland*

^q*University of Ljubljana, Ljubljana, Slovenia*

^r*University of Maribor, Maribor, Slovenia*

^s*University of Melbourne, Victoria, Australia*

^t*Nagoya University, Nagoya, Japan*

^u*National Central University, Chung-li, Taiwan*

^v*National United University, Miao Li, Taiwan*

^w*Department of Physics, National Taiwan University, Taipei, Taiwan*

^x*H. Niewodniczanski Institute of Nuclear Physics, Krakow, Poland*

^y*Nippon Dental University, Niigata, Japan*

^z*Niigata University, Niigata, Japan*

^{aa}*University of Nova Gorica, Nova Gorica, Slovenia*

^{ab}*Osaka City University, Osaka, Japan*

^{ac}*Osaka University, Osaka, Japan*

^{ad}*Panjab University, Chandigarh, India*

^{ae}*Peking University, Beijing, PR China*

^{af}*RIKEN BNL Research Center, Brookhaven, NY, USA*

^{ag}*University of Science and Technology of China, Hefei, PR China*

^{ah}*Seoul National University, Seoul, South Korea*

^{ai}*Sungkyunkwan University, Suwon, South Korea*

^{aj}*University of Sydney, Sydney, NSW, Australia*

^{ak}*Tata Institute of Fundamental Research, Mumbai, India*

^{al}*Toho University, Funabashi, Japan*

^{am}*Tohoku Gakuin University, Tagajo, Japan*

^{an}*Tohoku University, Sendai, Japan*

^{ao}*Department of Physics, University of Tokyo, Tokyo, Japan*

^{ap}*Tokyo Institute of Technology, Tokyo, Japan*

^{aq}*Tokyo Metropolitan University, Tokyo, Japan*

^{ar}*Tokyo University of Agriculture and Technology, Tokyo, Japan*

^{as}*Virginia Polytechnic Institute and State University, Blacksburg, VA, USA*

^{at}*Yonsei University, Seoul, South Korea*

Abstract

We report measurements and searches for resonant $B^\pm \rightarrow K^\pm h \rightarrow K^\pm \gamma\gamma$ decays where h is a η , η' , η_c , $\eta_c(2S)$, χ_{c0} , χ_{c2} , J/ψ meson or the $X(3872)$ particle. The results are based on a data sample containing 535 million $B\bar{B}$ pairs collected with the Belle detector at the KEKB e^+e^- asymmetric-energy collider operating at the $\Upsilon(4S)$ resonance. Signals are observed in the modes with η and η' , and we obtain evidence for a signal in the mode with η_c . We measure $\mathcal{B}(B^\pm \rightarrow K^\pm \eta \rightarrow K^\pm \gamma\gamma) = (0.87^{+0.16}_{-0.15}(\text{stat})^{+0.10}_{-0.07}(\text{syst})) \times 10^{-6}$, $\mathcal{B}(B^\pm \rightarrow K^\pm \eta' \rightarrow K^\pm \gamma\gamma) = (1.40^{+0.16}_{-0.15}(\text{stat})^{+0.15}_{-0.12}(\text{syst})) \times 10^{-6}$ and $\mathcal{B}(B^\pm \rightarrow K^\pm \eta_c \rightarrow K^\pm \gamma\gamma) = (0.22^{+0.09}_{-0.07}(\text{stat})^{+0.04}_{-0.02}(\text{syst})) \times 10^{-6}$. We set upper limits on the branching fractions of the other modes.

Key words: B, X(3872), charmonia

PACS: 13.25.Hw, 14.40.-n

1 Introduction

We report searches for resonant $B^\pm \rightarrow K^\pm h \rightarrow K^\pm \gamma\gamma$ decays, where h can be one of the following mesons: η , η' , η_c , $\eta_c(2S)$, χ_{c0} , χ_{c2} , J/ψ or the $X(3872)$ [1,2,3,4] particle. Many of the $B^\pm \rightarrow K^\pm h$ and $h \rightarrow \gamma\gamma$ branching fractions involved in these decay chains have been already measured, as shown in Table 1. The $B^\pm \rightarrow K^\pm \eta$ and $B^\pm \rightarrow K^\pm \eta'$ modes are well established [5] and can be used as calibrations in the search for other $B^\pm \rightarrow K^\pm h \rightarrow K^\pm \gamma\gamma$ channels that have lower or unknown branching fractions. The $B^\pm \rightarrow K^\pm J/\psi$ channel can also serve as a control mode, since the decay of a spin 1 particle (here the J/ψ) into two photons is forbidden by gauge invariance and Bose-Einstein statistics [6].

The nature and quantum numbers of the $X(3872)$ particle are still being debated; based on analyses of the dipion mass spectrum [8,9] and angular distributions [8,10] for $X(3872) \rightarrow \pi^+ \pi^- J/\psi$, $J^{PC} = 1^{++}$ and 2^{-+} are allowed. The 1^{++} assignment is also supported by signals observed in $B \rightarrow (D^0 \bar{D}^0 \pi^0) K$ [9] and in $B \rightarrow (D^{*0} \bar{D}^0) K$ [11] under the assumption that they are indeed due to the $X(3872)$ particle. The observation of $X(3872) \rightarrow J/\psi \rho$ [12] and $X(3872) \rightarrow J/\psi \gamma$ [13,14] indicates that $C = +1$. Evidence of a signal in the $B^\pm \rightarrow K^\pm X(3872) \rightarrow K^\pm \gamma\gamma$ channel would rule out $J = 1$.

The interference of $B^\pm \rightarrow K^\pm \eta_c \rightarrow K^\pm \gamma\gamma$ or $B^\pm \rightarrow K^\pm \chi_{c0} \rightarrow K^\pm \gamma\gamma$ with the radiative decay chain $B^\pm \rightarrow K^{*\pm} \gamma \rightarrow K^\pm \gamma\gamma$ can be used to measure the photon polarization in the $b \rightarrow s\gamma$ quark transition [15]. Such measurement would provide a test of the Standard Model, which predicts the photon to be predominantly left-handed in $b \rightarrow s\gamma$ decays and right-handed in $\bar{b} \rightarrow \bar{s}\gamma$ decays. The observation of the $B^\pm \rightarrow K^\pm \eta_c \rightarrow K^\pm \gamma\gamma$ or $B^\pm \rightarrow K^\pm \chi_{c0} \rightarrow K^\pm \gamma\gamma$ decay chain is the first step in this search for new physics, which could be achieved with about 10 ab^{-1} of data (thus requiring a Super B factory). The non-resonant decay $B^\pm \rightarrow K^\pm \gamma\gamma$ is very rare, with a branching fraction estimated to be of order 10^{-9} [16] with a large background over the whole $m_{\gamma\gamma}$ phase-space from the resonant $B^\pm \rightarrow K^{*\pm} \gamma \rightarrow K^\pm \gamma\gamma$ channel [15].

In this study, we use a data sample of 492 fb^{-1} containing $535 \times 10^6 B\bar{B}$ pairs that were collected with the Belle detector at the KEKB asymmetric-energy $e^+ e^-$ (3.5 on 8 GeV) collider [17] operating at the $\Upsilon(4S)$ resonance.

The Belle detector is a large-solid-angle magnetic spectrometer that consists of a silicon vertex detector (SVD), a 50-layer central drift chamber (CDC), an array of aerogel threshold Cherenkov counters (ACC), a barrel-like arrangement of time-of-flight scintillation counters (TOF), and an electromagnetic calorimeter comprised of CsI(Tl) crystals (ECL) located inside a superconducting solenoid coil that provides a 1.5 T magnetic field. An iron flux-return

Table 1

Current status of the measured branching fractions or 90% confidence level upper limits for $B^\pm \rightarrow K^\pm h$ and $h \rightarrow \gamma\gamma$ (all values are taken from Ref. [5], unless otherwise indicated). The values in the last column are the expectations computed as the products $\mathcal{B}(B^\pm \rightarrow K^\pm h) \times \mathcal{B}(h \rightarrow \gamma\gamma)$. The decay chain $B^\pm \rightarrow K^\pm h \rightarrow K^\pm \gamma\gamma$ has only been observed for $h = \eta$.

h	$\mathcal{B}(B^\pm \rightarrow K^\pm h)$	$\mathcal{B}(h \rightarrow \gamma\gamma)$	$\mathcal{B}(B^\pm \rightarrow K^\pm h \rightarrow K^\pm \gamma\gamma)$
η	$(2.6 \pm 0.6) \times 10^{-6}$	$(39.39 \pm 0.24)\%$	$(1.02 \pm 0.24) \times 10^{-6}$
η'	$(69.7 \pm 2.8) \times 10^{-6}$	$(2.12 \pm 0.14)\%$	$(1.48 \pm 0.11) \times 10^{-6}$
η_c	$(9.1 \pm 1.3) \times 10^{-4}$	$(2.7 \pm 0.9) \times 10^{-4}$	$(0.25 \pm 0.09) \times 10^{-6}$
$\eta_c(2S)$	$(3.4 \pm 1.8) \times 10^{-4}$	seen	
χ_{c0}	$(1.40^{+0.23}_{-0.19}) \times 10^{-4}$	$(2.76 \pm 0.33) \times 10^{-4}$	$(0.39 \pm 0.08) \times 10^{-7}$
χ_{c2}	$< 2.9 \times 10^{-5}$	$(2.58 \pm 0.19) \times 10^{-4}$	$< 7.5 \times 10^{-9}$
J/ψ	$(10.07 \pm 0.35) \times 10^{-4}$	$< 9.3 \times 10^{-5}$ [7]	$< 9.4 \times 10^{-8}$
$X(3872)$	seen [1]		

located outside the coil is instrumented to detect K_L^0 mesons and to identify muons (KLM). The detector is described in detail elsewhere [18]. Two inner detector configurations were used. A 2.0 cm beampipe and a 3-layer silicon vertex detector was used for the first sample of $152 \times 10^6 B\bar{B}$ pairs (SVD1), while a 1.5 cm beampipe, a 4-layer silicon detector and a small-cell inner drift chamber were used to record the remaining $383 \times 10^6 B\bar{B}$ pairs (SVD2 [19]).

2 Event selection and background rejection

Kaon candidates are selected from charged tracks with the requirement $\mathcal{L} = \mathcal{L}_K/(\mathcal{L}_K + \mathcal{L}_\pi) > 0.6$, where \mathcal{L}_K (\mathcal{L}_π) is the likelihood for a track to be a kaon (pion) based on the response of the ACC and on measurements from the CDC and TOF. The kaon identification efficiency is between 84% and 90% depending on the $K\gamma\gamma$ signal mode with 7%–11% of pions misidentified as kaons. Photon pairs are selected by requiring their energies in the laboratory frame to be greater than 100 MeV and their energy asymmetry $A_{\gamma\gamma} = |\frac{E_{\gamma 1} - E_{\gamma 2}}{E_{\gamma 1} + E_{\gamma 2}}|$ to be less than 0.9. We reject photons from π^0 decays by removing photon pairs with an invariant mass between 117.8 MeV/ c^2 and 150.2 MeV/ c^2 (2.5 standard deviations around the π^0 mass). We require a shower shape consistent with that of a photon: for each cluster, the ratio of the energy deposited in the array of the central 3×3 calorimeter cells to that of 5×5 cells is computed. The cluster associated with the most energetic photon of the candidate pair is required to have a ratio greater than 0.95 while the cluster from the other

Table 2

Nominal mass [GeV/c^2] of the reconstructed particles and definition of invariant mass windows [GeV/c^2] for photon pairs and of the ΔE signal windows [GeV]. The M_{bc} signal windows are defined as $M_{bc} > 5.27 \text{ GeV}/c^2$ for all modes.

Particle	Mass	Wide $m_{\gamma\gamma}$ win.	Tight $m_{\gamma\gamma}$ win.	ΔE win.
η	0.548	0.4–0.7	0.50–0.57	$-0.15 < \Delta E < 0.10$
η'	0.958	0.8–1.1	0.90–0.98	$-0.15 < \Delta E < 0.10$
η_c	2.980	2.5–3.2	2.82–3.05	$-0.10 < \Delta E < 0.10$
$\eta_c(2S)$	3.637	3.2–3.8	3.44–3.70	$-0.08 < \Delta E < 0.06$
χ_{c0}	3.415	3.0–3.5	3.25–3.50	$-0.10 < \Delta E < 0.10$
χ_{c2}	3.556	3.0–3.8	3.40–3.62	$-0.06 < \Delta E < 0.06$
J/ψ	3.097	2.5–3.2	2.92–3.15	$-0.09 < \Delta E < 0.09$
$X(3872)$	3.872	3.0–4.1	3.72–3.95	$-0.09 < \Delta E < 0.09$

photon must have a ratio greater than 0.90 for the $B^\pm \rightarrow K^\pm \eta$ and $B^\pm \rightarrow K^\pm \eta'$ channels and 0.95 for the other channels.

Pairs of photons are retained and associated to the corresponding meson when their invariant mass ($m_{\gamma\gamma}$) is inside one of the *wide* mass windows defined in Table 2. A mass-constrained fit of the photon momenta is performed to match the nominal [5] masses with the constraint that the photons originate from the interaction point.

Charged B meson candidates are reconstructed starting from a kaon and a pair of photons, and they are selected by means of the beam-energy constrained mass, defined as $M_{bc} = \sqrt{E_{\text{beam}}^{*2} - p_B^{*2}}$ and the energy difference $\Delta E = E_B^* - E_{\text{beam}}^*$. In these definitions, E_{beam}^* is the beam energy and p_B^* and E_B^* are the momentum and the energy of the B meson, all variables being evaluated in the center-of-mass (CM) frame. We select B -meson candidates with $M_{bc} > 5.2 \text{ GeV}/c^2$ and $-0.3 \text{ GeV} < \Delta E < 0.3 \text{ GeV}$. If more than one B candidate is reconstructed in an event, the best candidate is chosen by selecting the photon pair with the smallest χ^2 of the mass fit, and if multiple kaons can be associated with this photon pair, the kaon with the highest \mathcal{L} is chosen.

The main background in all modes is due to continuum events, i.e. events coming from light-quark pair production ($u\bar{u}$, $d\bar{d}$, $s\bar{s}$ and $c\bar{c}$). The rejection of the continuum is studied and optimized using a Monte Carlo (MC) sample having about 1.5 times the size of the data sample. Four variables are used to separate signal from continuum background: a Fisher discriminant based on modified Fox-Wolfram moments [20], the B production angle with respect to the beam in the CM frame, $\cos\theta^*$, the flight length difference along the beam axis between the two B mesons, and the flavor tagging information [21]. The Fisher

Table 3

Signal efficiencies for the two configurations of the detector.

Particle	$\epsilon(\text{SVD1}) [\%]$	$\epsilon(\text{SVD2}) [\%]$
η	15.8 ± 0.1	16.6 ± 0.1
η'	14.6 ± 0.1	15.7 ± 0.1
η_c	10.0 ± 0.1	10.9 ± 0.1
$\eta_c(2S)$	10.9 ± 0.1	11.4 ± 0.1
χ_{c0}	11.0 ± 0.1	11.6 ± 0.1
χ_{c2}	10.4 ± 0.1	11.3 ± 0.1
J/ψ	9.4 ± 0.1	9.7 ± 0.1
$X(3872)$	13.7 ± 0.1	15.0 ± 0.1

discriminant, the B production angle and the flight length difference are combined into a likelihood ratio $LR = L_s/(L_s + L_{udsc})$, where L_s and L_{udsc} are the product of probability density functions (PDFs) of these variables for signal and continuum events. We use different LR cuts depending on the flavor tagging information. The continuum rejection is achieved by simultaneously optimizing the LR and $m_{\gamma\gamma}$ cuts (*tight* $m_{\gamma\gamma}$ window in Table 2) in order to maximize the figure of merit in the signal windows ($M_{bc} > 5.27 \text{ GeV}/c^2$ and ΔE as described in Table 2). The figure of merit is defined as $\mathcal{S} = N_s/\sqrt{N_s + N_{udsc}}$ for the $B^\pm \rightarrow K^\pm \eta$ and $B^\pm \rightarrow K^\pm \eta'$ modes and $\epsilon/\sqrt{N_{udsc}}$ for all the other modes, where N_s and N_{udsc} are the expected number of signal and continuum events and ϵ is the signal efficiency. The expected numbers of events are computed for an integrated luminosity of 492 fb^{-1} and assuming the measured branching fractions [5].

Exclusive backgrounds from charmless B decays are studied using large MC samples having about 36 times the size of the data sample. In the $B^\pm \rightarrow K^\pm \eta$ channel, 56% of this type of background is from $B \rightarrow K^* \eta$ with the rest being composed of several small contributions, the largest ones being due to $B \rightarrow X_s \gamma$ and $B^\pm \rightarrow \eta \pi^\pm$. In the $B^\pm \rightarrow K^\pm \eta'$ channel, the dominant source (about 2/3) is $B \rightarrow X_s \gamma$, about half of which is from $B \rightarrow K^*(K\pi)\gamma$. For the other modes, about 95% of the charmless B decay contributions is due to $B \rightarrow X_s \gamma$. The final state with $K^\pm \pi^0 \gamma$ is a significant background for modes with charmonia and with the $X(3872)$ resonance. It is suppressed by the requirement $m_{K\gamma_2} > 1.5 \text{ GeV}/c^2$, where $m_{K\gamma_2}$ is the invariant mass of the system formed by the kaon and the lowest energy photon (in the laboratory frame) forming the $K\gamma\gamma$ candidate. For the $B^\pm \rightarrow K^\pm \eta_c$ channel, the $B \rightarrow K^*(892)\eta_c(\gamma\gamma)$ background is the most relevant contribution.

Another source of background is produced by the overlap of a hadronic event with a previous QED interaction (mainly Bhabha scattering) that has left

energy deposits in the calorimeter. This off-time background is removed by using the timing information of the calorimeter clusters corresponding to each photon candidate. This timing information is only available for the most recent data, containing $258 \times 10^6 B\bar{B}$ pairs. For the rest of the data, we include the background in the fit described in the following section, by modeling it according to the off-time background events rejected from the most recent data.

The tight $m_{\gamma\gamma}$ windows overlap for some of the h decays, e.g. the mass window for η_c includes some candidates for J/ψ and vice versa. Dedicated studies have shown that, for the dataset considered in this analysis, the only non-negligible cross-feed is due to $B^\pm \rightarrow K^\pm \eta_c$ events that are reconstructed in the $B^\pm \rightarrow K^\pm J/\psi$ mode. This effect is included in the fit as described below.

The signals are described using PDFs modeled by the product of a Crystal Ball function [22] for M_{bc} and three Gaussian functions for ΔE . The shapes and efficiencies are determined from an extended unbinned two-dimensional (M_{bc} and ΔE) fit to MC signal events merged into toy continuum events modeled by an ARGUS [23] function for M_{bc} and a first order polynomial function for ΔE . The M_{bc} resolution and the ΔE resolution and mean for the signal are corrected using a control sample of $B^\pm \rightarrow K^\pm \pi^0$ events. Table 3 lists the efficiencies obtained for all reconstructed modes in the two sub-samples with different inner detector configurations.

3 Fitting procedure and results

We perform a two-dimensional unbinned extended maximum likelihood fit to M_{bc} and ΔE . The signal and continuum background PDFs are those described in the previous section. The $B\bar{B}$ and off-time backgrounds are modeled with two-dimensional KEYS [24] PDFs extracted from MC events and from the off-time data sample, respectively. The normalizations of the $B\bar{B}$ and off-time backgrounds are fixed in the fit. For the $B^\pm \rightarrow K^\pm J/\psi$ mode, the $K^\pm \eta_c$ cross-feed is included with normalization fixed to the value obtained in the corresponding signal fit.

The fit is performed for M_{bc} greater than 5.2 GeV/ c^2 and for ΔE between -0.3 GeV and 0.3 GeV. The likelihood is defined as :

$$\mathcal{L} = e^{-\sum_j N_j} \times \prod_i \left(\sum_j N_j P_j^i(M_{bc}^i, \Delta E^i) \right) \quad (1)$$

where i runs over all events, j runs over the possible event categories (signal, continuum background and other backgrounds), N_j is the number of events in each category and P_j is the corresponding PDF.

Table 4

Systematic uncertainties on the detection efficiency related to particle reconstruction and identification and to signal selection requirements.

Source	Uncertainty [%]
Photon reconstruction efficiency	2×2.2
Tracking efficiency	1×1
Kaon identification efficiency	2
$m_{\gamma\gamma}$ cut efficiency	3.6
LR cut efficiency	6.9
Total	9.2

The data are divided into sub-samples based on the SVD configuration and the availability of the timing information needed for the rejection of off-time background.

The fit variables are the branching fraction (\mathcal{B}) and the continuum background normalization and PDF parameters, except the ARGUS endpoint which is fixed to $E_{\text{beam}}^* = 5.289$ GeV. The number of signal events is then defined as $S^k = \mathcal{B} \times \epsilon^k \times N_{B\bar{B}}^k$ where $N_{B\bar{B}}^k$ is the number of $B\bar{B}$ events and ϵ^k is the signal efficiency, both evaluated for sub-sample k .

The branching fraction obtained from the fit depends on the following parameters that can give rise to systematic uncertainties:

- (1) signal PDF parameters (0–5% uncertainty),
- (2) signal efficiency (1% uncertainty due to limited MC statistics),
- (3) normalization of the charmless B and off-time backgrounds and of the $K^\pm \eta_c$ cross-feed for the $B^\pm \rightarrow K^\pm J/\psi$ mode (1–10%),
- (4) number of $B\bar{B}$ events (1.3%),
- (5) parameters related to particle reconstruction and identification and to signal selection that affect the signal in the same way for all sub-samples, as summarized in Table 4.

Systematic uncertainties related to the $m_{\gamma\gamma}$ and LR requirements are evaluated by comparing efficiencies in data and MC using a $B^\pm \rightarrow K^\pm \pi^0$ control sample. Systematic uncertainties are included in the likelihood function by integration. The statistical likelihood is convolved with the probability distribution of the systematics parameters listed above, computed as the product of Gaussian terms, one for each parameter. A MC integration is performed over the phase space of the systematics parameters, yielding a new likelihood function, $\mathcal{L}_{\text{syst}}$, that includes all systematic uncertainties. The fit results quoted below are all extracted from $\mathcal{L}_{\text{syst}}$. The central value \mathcal{B}_0 is the \mathcal{B} at which $\mathcal{L}_{\text{syst}}$

has its maximum and the errors $\delta_{\text{tot}}^{\pm}$ are defined by :

$$\frac{\int_{\mathcal{B}_0 + \delta_{\text{tot}}^-}^{\mathcal{B}_0 + \delta_{\text{tot}}^+} \mathcal{L}_{\text{syst}} d\mathcal{B}}{\int_0^1 \mathcal{L}_{\text{syst}} d\mathcal{B}} = 0.68 \quad (2)$$

where the integration interval is chosen such that all points outside the interval have a lower likelihood than those inside. The positive (negative) systematic error is computed as $\pm \sqrt{\delta_{\text{tot}}^{\pm 2} - \delta_{\text{stat}}^{\pm 2}}$ where $\delta_{\text{stat}}^{\pm}$ is the positive (negative) statistical error. The significance of the measurement of the branching fraction is defined as $\sqrt{2(\ln \mathcal{L}_{\text{syst}}(\mathcal{B} = \mathcal{B}_0) - \ln \mathcal{L}_{\text{syst}}(\mathcal{B} = 0))}$. For modes in which no significant signal is found, the 90% confidence level (CL) upper limit, $\mathcal{B}_{\text{limit}}$, is computed by likelihood integration, according to:

$$\frac{\int_0^{\mathcal{B}_{\text{limit}}} \mathcal{L}_{\text{syst}} d\mathcal{B}}{\int_0^1 \mathcal{L}_{\text{syst}} d\mathcal{B}} = 0.9 \quad (3)$$

The fit results for all modes are summarized in Table 5. We observe signals in the $B^{\pm} \rightarrow K^{\pm}\eta$ and $B^{\pm} \rightarrow K^{\pm}\eta'$ modes and obtain evidence for a signal in the $B^{\pm} \rightarrow K^{\pm}\eta_c$ channel, while we see no signal in the other modes. We report the first measurements of $B^{\pm} \rightarrow K^{\pm}\eta'$ and $B^{\pm} \rightarrow K^{\pm}\eta_c$ channels in the $K^{\pm}\gamma\gamma$ final state. We measure $\mathcal{B}(B^{\pm} \rightarrow K^{\pm}\eta \rightarrow K^{\pm}\gamma\gamma) = (0.87^{+0.16}_{-0.15}(\text{stat})^{+0.10}_{-0.07}(\text{syst})) \times 10^{-6}$ in agreement with Belle's measurement of this mode with the same dataset [25], $\mathcal{B}(B^{\pm} \rightarrow K^{\pm}\eta' \rightarrow K^{\pm}\gamma\gamma) = (1.40^{+0.16}_{-0.15}(\text{stat})^{+0.15}_{-0.12}(\text{syst})) \times 10^{-6}$ and $\mathcal{B}(B^{\pm} \rightarrow K^{\pm}\eta_c \rightarrow K^{\pm}\gamma\gamma) = (0.22^{+0.09}_{-0.07}(\text{stat})^{+0.04}_{-0.02}(\text{syst})) \times 10^{-6}$. All measured branching fractions agree with the values shown in the third column of Table 1. Fit projections are shown in Figures 1 and 2; in each plot the variable that is not shown is restricted to be in the signal window.

For the modes where no significant signal is observed, we extract the following 90% CL upper limits: $\mathcal{B}(B^{\pm} \rightarrow K^{\pm}\eta_c(2S) \rightarrow K^{\pm}\gamma\gamma) < 0.18 \times 10^{-6}$, $\mathcal{B}(B^{\pm} \rightarrow K^{\pm}\chi_{c0} \rightarrow K^{\pm}\gamma\gamma) < 0.11 \times 10^{-6}$, $\mathcal{B}(B^{\pm} \rightarrow K^{\pm}\chi_{c2} \rightarrow K^{\pm}\gamma\gamma) < 0.09 \times 10^{-6}$, $\mathcal{B}(B^{\pm} \rightarrow K^{\pm}J/\psi \rightarrow K^{\pm}\gamma\gamma) < 0.16 \times 10^{-6}$ and $\mathcal{B}(B^{\pm} \rightarrow K^{\pm}X(3872) \rightarrow K^{\pm}\gamma\gamma) < 0.24 \times 10^{-6}$. Whenever the branching fraction of $B^{\pm} \rightarrow K^{\pm}h$ has been measured elsewhere, we also perform the fit by constraining $\mathcal{B}(B^{\pm} \rightarrow K^{\pm}h)$ to the measured value [5], thus extracting an upper limit on $\mathcal{B}(h \rightarrow \gamma\gamma)$. The uncertainty on $\mathcal{B}(B^{\pm} \rightarrow K^{\pm}h)$ is included as a source of systematic uncertainty. We obtain $\mathcal{B}(\chi_{c0} \rightarrow \gamma\gamma) < 9.5 \times 10^{-4}$, $\mathcal{B}(\eta_c(2S) \rightarrow \gamma\gamma) < 8.2 \times 10^{-4}$ and $\mathcal{B}(J/\psi \rightarrow \gamma\gamma) < 1.6 \times 10^{-4}$ at 90% CL. Similarly, for the $B^{\pm} \rightarrow K^{\pm}\eta_c$ mode, we determine $\mathcal{B}(\eta_c \rightarrow \gamma\gamma) = (2.4^{+0.9}_{-0.8}(\text{stat})^{+0.7}_{-0.4}(\text{syst})) \times 10^{-4}$.

The absolute branching fraction $\mathcal{B}(B^{\pm} \rightarrow K^{\pm}X(3872))$ has not yet been measured. However, there are measurements of the product of this quantity and the branching fractions of different decays of the $X(3872)$. Assuming that $X(3872)$ decays to $J/\psi\pi^+\pi^-$, $J/\psi\pi^+\pi^-\pi^0$ and $J/\psi\gamma$ saturate all possible decays of the

Table 5

Signal yields, branching fractions and significances (\mathcal{S}) results for $B^\pm \rightarrow K^\pm h \rightarrow K^\pm \gamma\gamma$. The first uncertainty is statistical, the second one is systematic. Limits are calculated at 90% confidence level.

Resonance	Yield	$\mathcal{B}(B^\pm \rightarrow K^\pm h \rightarrow K^\pm \gamma\gamma) (10^{-6})$	\mathcal{S}	$\mathcal{B}(h \rightarrow \gamma\gamma)$
η	76^{+14}_{-13}	$0.87^{+0.16+0.10}_{-0.15-0.07}$	7.3	$(31.0^{+5.6+7.6}_{-5.3-7.1})\%$
η'	114 ± 13	$1.40^{+0.16+0.15}_{-0.15-0.12}$	13.8	$(2.01^{+0.23+0.23}_{-0.22-0.19})\%$
η_c	$13.3^{+4.8}_{-4.1}$	$0.22^{+0.09+0.04}_{-0.07-0.02}$	4.1	$(2.4^{+0.9+0.7}_{-0.8-0.4}) \times 10^{-4}$
$\eta_c(2S)$	$4.0^{+3.9}_{-3.0}$	< 0.18	—	$< 8.2 \times 10^{-4}$
χ_{c0}	$0.7^{+2.5}_{-1.7}$	< 0.11	—	$< 9.5 \times 10^{-4}$
χ_{c2}	$-0.3^{+2.6}_{-1.9}$	< 0.09	—	—
J/ψ	$3.4^{+2.8}_{-2.0}$	< 0.16	—	$< 1.6 \times 10^{-4}$
$X(3872)$	$-0.9^{+2.2}_{-1.4}$	< 0.24	—	$< 1.1\%$

$X(3872)$ and taking the values of the corresponding products from [5,13,14], we derive a conservative upper limit $\mathcal{B}(X(3872) \rightarrow \gamma\gamma) < 1.1\%$ at 90% CL.

4 Conclusions

A search for resonant $B^\pm \rightarrow K^\pm h \rightarrow K^\pm \gamma\gamma$ decays, where the resonance h can be $\eta, \eta', \eta_c, \eta_c(2S), \chi_{c0}, \chi_{c2}, J/\psi$ or $X(3872)$, has been performed in a sample containing 535 million $B\bar{B}$ pairs. We have observed $B^\pm \rightarrow K^\pm \eta$ and $B^\pm \rightarrow K^\pm \eta'$ with significances of 7.3 and 13.8, respectively, and we have obtained evidence for $B^\pm \rightarrow K^\pm \eta_c$ with a significance of 4.1. No evidence of a signal is observed in any of the other modes and 90% CL upper limits are set on the corresponding branching fractions. The measured branching fraction for $B^\pm \rightarrow K^\pm \eta \rightarrow K^\pm \gamma\gamma$ is in agreement with Belle's measurement of this mode with the same dataset [25]. We report the first observation of $B^\pm \rightarrow K^\pm \eta'$ and the first evidence of $B^\pm \rightarrow K^\pm \eta_c$ in the $K^\pm \gamma\gamma$ final state.

We thank the KEKB group for the excellent operation of the accelerator, the KEK cryogenics group for the efficient operation of the solenoid, and the KEK computer group and the National Institute of Informatics for valuable computing and Super-SINET network support. We acknowledge support from the Ministry of Education, Culture, Sports, Science, and Technology of Japan and the Japan Society for the Promotion of Science; the Australian Research Council and the Australian Department of Education, Science and Training; the National Science Foundation of China under contract No. 10575109 and 10775142; the Department of Science and Technology of India; the BK21 program of the Ministry of Education of Korea, the CHEP SRC program and Ba-

sic Research program (grant No. R01-2005-000-10089-0) of the Korea Science and Engineering Foundation, and the Pure Basic Research Group program of the Korea Research Foundation; the Polish State Committee for Scientific Research; the Ministry of Education and Science of the Russian Federation and the Russian Federal Agency for Atomic Energy; the Slovenian Research Agency; the Swiss National Science Foundation; the National Science Council and the Ministry of Education of Taiwan; and the U.S. Department of Energy.

References

- [1] S.-K. Choi, S.L. Olsen *et al.* (Belle Collab.), Phys. Rev. Lett. **91**, 262001 (2003).
- [2] D. Acosta *et al.* (CDF Collab.), Phys. Rev. Lett. **93**, 072001 (2004).
- [3] V.M. Abazov *et al.* (D0 Collab.), Phys. Rev. Lett. **93**, 162002 (2004).
- [4] A. Aubert *et al.* (BaBar Collab.), Phys. Rev. D **71**, 071103 (2005).
- [5] W.-M. Yao *et al.* (Particle Data Group), J. Phys. G **33**, 1 (2006) and 2007 partial update for the 2008 edition.
- [6] L.D. Landau, Dokl. Akad. Nauk USSR **60**, 207 (1948) and Phys. Abstracts A52, 125 (1949).
C.N. Yang, Phys. Rev. **77**, 242 (1950).
- [7] R. Brandelik *et al.* (DASP Collab.), Z. Phys. C **1**, 233 (1979).
- [8] K. Abe *et al.* (Belle Collab.), arXiv:hep-ex/0505038 (2005).
- [9] G. Gokhroo, G. Majumder *et al.* (Belle Collab.), Phys. Rev. Lett. **97**, 162002 (2006).
- [10] A. Abulencia *et al.* (CDF Collab.), Phys. Rev. Lett. **98**, 132002 (2007).
- [11] A. Aubert *et al.* (BaBar Collab.), arXiv:0708.1565 (2007).
- [12] A. Abulencia *et al.* (CDF Collab.), Phys. Rev. Lett. **96**, 102002 (2006).
- [13] K. Abe *et al.* (Belle Collab.), arXiv:hep-ex/0505037 (2005).
- [14] A. Aubert *et al.* (BaBar Collab.), Phys. Rev. D **74**, 071101 (2006).
- [15] M. Knecht and T. Schietinger, Phys. Lett. B **634**, 403 (2006).
- [16] G. Hiller and A.S. Safir, JHEP **0502**, 011 (2005).
See also: S.R. Choudhury, G.C. Joshi, N. Mahajan and B.H.J. McKellar, Phys. Rev. D **67**, 074016 (2003); erratum: Phys. Rev. D **72**, 119906 (2005).
- [17] S. Kurokawa and E. Kikutani, Nucl. Instr. and Meth. A **499**, 1 (2003) and other papers included in this volume.

- [18] A. Abashian *et al.* (Belle Collab.), Nucl. Instr. and Meth. A **479**, 117 (2002).
- [19] Z. Natkaniec *et al.* (Belle SVD2 Group), Nucl. Instr. and Meth. A **560**, 1 (2006).
- [20] The Fox-Wolfram moments were introduced in G.C. Fox and S. Wolfram, Phys. Rev. Lett. **41**, 1581 (1978). The Fisher discriminant used by Belle, based on modified Fox-Wolfram moments, is described in K. Abe *et al.* (Belle Collab.), Phys. Rev. Lett. **87**, 101801 (2001) and K. Abe *et al.* (Belle Collab.), Phys. Lett. B **511**, 151 (2001).
- [21] H. Kakuno *et al.*, Nucl. Instr. and Meth. A **533**, 516 (2004).
- [22] J.E. Gaiser *et al.* (Crystal Ball Collab.), Phys. Rev. D **34**, 711 (1986).
- [23] H. Albrecht *et al.* (ARGUS Collab.), Phys. Lett. B **185**, 218 (1987).
- [24] K.S. Cranmer, Comput. Phys. Commun. **136**, 198 (2001).
- [25] P. Chang *et al.* (Belle Collab.), Phys. Rev. D **75**, 071104 (2007).

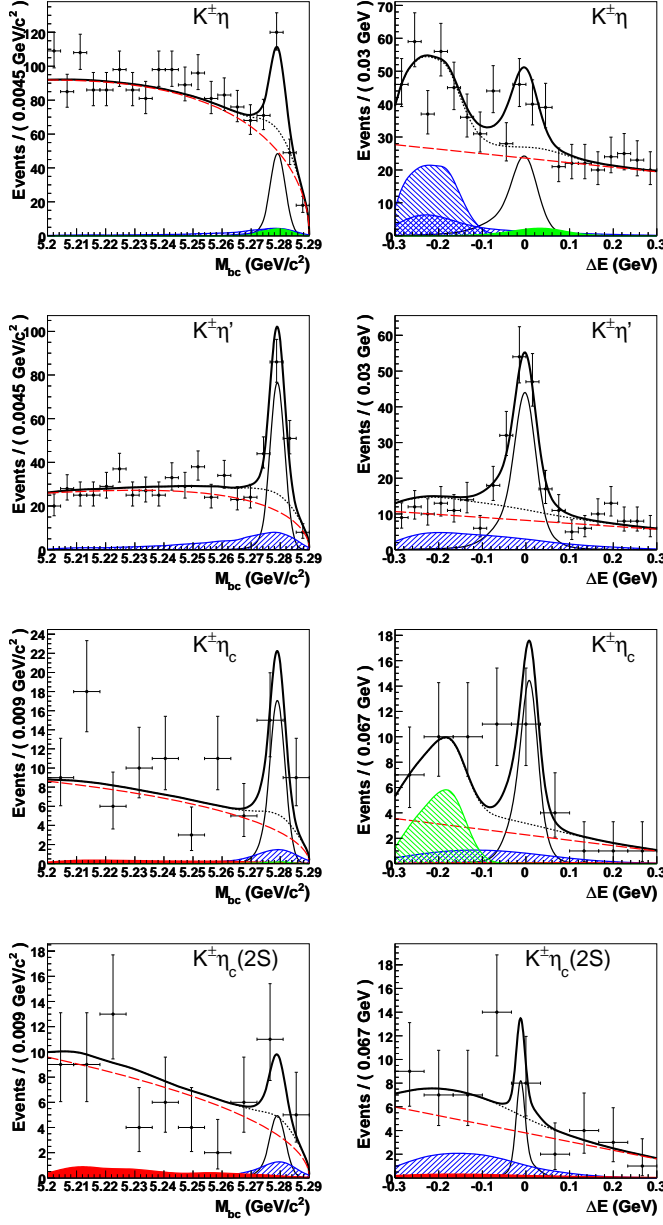


Fig. 1. M_{bc} and ΔE projections together with fit results. The first row presents the $B^\pm \rightarrow K^\pm \eta$ mode, the second one $B^\pm \rightarrow K^\pm \eta'$, the third one $B^\pm \rightarrow K^\pm \eta_c$ and the last one $B^\pm \rightarrow K^\pm \eta_c(2S)$. The points with error bars represent data, the thick solid curves are the fit functions, the thin solid curve is the signal function, the dashed curves show the continuum contribution and the dotted curves show the sum of all background contributions. The hatched area present in the whole ΔE region is the contribution from the charmless B decays. The hatched area around $\Delta E = -0.2$ GeV in $B^\pm \rightarrow K^\pm \eta$ ($B^\pm \rightarrow K^\pm \eta_c$) shows the contribution from $B \rightarrow K^* \eta$ decays ($B \rightarrow K^* \eta_c$). The filled area around $\Delta E = 0.05$ GeV in the $B^\pm \rightarrow K^\pm \eta$ plot is the contribution from $B^\pm \rightarrow \pi^\pm \eta$. The filled area in $B^\pm \rightarrow K^\pm \eta_c(2S)$ is the contribution from the off-time background.

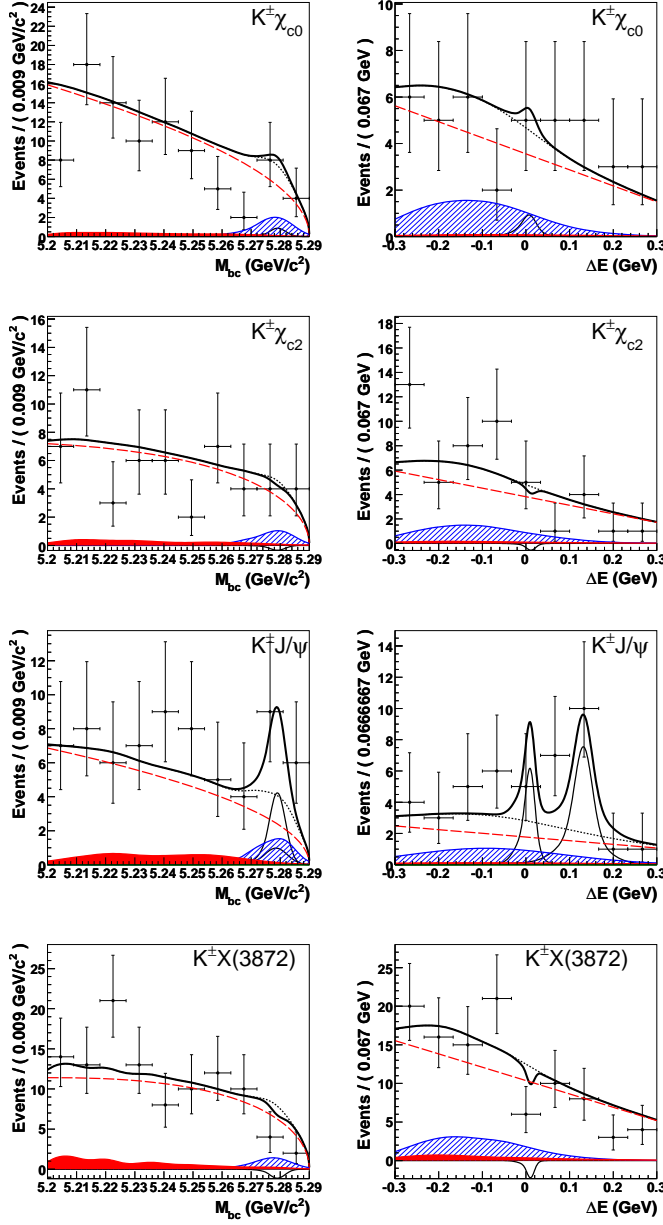


Fig. 2. M_{bc} and ΔE projections together with fit results. The first row presents the $B^\pm \rightarrow K^\pm \chi_{c0}$ mode, the second one $B^\pm \rightarrow K^\pm \chi_{c2}$, the third one $B^\pm \rightarrow K^\pm J/\psi$ and the last one $B^\pm \rightarrow K^\pm X(3872)$. The points with error bars represent data, the thick solid curves are the fit functions, the thin solid curve is the signal function, the dotted curves show the sum of all background contributions, the dashed curves show the continuum contribution, the hatched areas are the contribution from the charmless B decays and the filled areas the contribution from the off-time background. In the $B^\pm \rightarrow K^\pm J/\psi$ plots, the $B^\pm \rightarrow K^\pm \eta_c$ cross-feed is visible in the thin solid curves as a small peaking background in M_{bc} that is concentrated around 120 MeV in ΔE .